Article

A Global Search Algorithm for Determining Water Influx in Naturally Fractured Reservoirs

Jiali Zhang [1], Xinwei Liao [1], Zhiming Chen [1,* and Nutao Wang [2]

[1] State Key Laboratory of Petroleum Resources and Prospecting, China University of Petroleum (Beijing), Beijing 102249, China

[2] State Key Laboratory of Oil and Gas Reservoir Geology and Exploitation, Southwest Petroleum University, Chengdu 610500, China

* Correspondence: zhimingchn@cup.edu.cn; Tel.: +86-1881-090-5983

check for updates

Abstract: The determination of water influx in naturally fractured reservoirs is always a significant and difficult task in gas reservoir engineering. To improve this situation, this paper presents a new global search algorithm to determine water influx in the naturally fractured gas reservoirs. In the methodology, a dimensionless water influx derivative curve is first introduced in this paper. It is used to identify flow regimes of water invasion by combining with the water influx characteristic curve. Following that, a sensitivity analysis is performed to study the impacts of key factors on flow regimes. Finally, based on the sensitivity study and material balance equation, a global search algorithm is proposed to obtain water influx. Results show that there are two steps in the dimensionless water influx curve and a "V-shape" in the derivative curve. The smaller the aquifer and gas reservoir radius ratio is, the earlier and more obvious the "V-shape" appears. The smaller the storativity ratio is, the earlier the "V-shape" appears. The smaller the interporosity flow coefficient is, the more obvious the "V-shape" is. Results of the field application demonstrate the method applicability, which provide a good reference for further work about determination of water influx.

Keywords: naturally fractured reservoirs; water influx; new method; material balance equation; case study

1. Introduction

Almost every gas reservoir is connected with a water body. When the water body is large and water invasion is strong during gas reservoir exploitation, and water influx becomes an indispensable parameter in the material balance equation of the gas reservoir, the calculation of water influx is particularly important. As it is impossible to monitor the water invasion directly, the determination of water influx in naturally fractured reservoirs has always been a difficult task in gas reservoir engineering. In the current research on water invasion, many scholars have established a steady-state, unsteady-state and pseudo-steady-state water invasion model for homogeneous gas reservoirs, which are mainly solved by the material balance method, statistical formula method and numerical simulation method [1–14].

Hu [3] determined the water saturation of gas reservoirs according to the pseudo-steady state water invasion model, so as to calculate the dynamic reserves. Combined with the principle of material balance, water influx was solved with the relationship between water influx and dynamic reserves. Furthermore, considering the presence of uncertainty in pressures, Mcewen [14] proposed a new and valuable method to calculate water influx based on the material balance equation.

Some scholars have developed some methods to determine water influx [15–18]. In 2007, Kryuchkov et al. [16] proposed using microscopic computer tomography technology to detect water

invasion, which avoids the tedious process of solving mathematical models. The method was simple and reliable, but the cost was high. In 2012, Al-Ghanim [15] proposed a nonparametric optimal transformations method to predict the water influx in the edge water drive reservoirs. This method can directly calculate water influx without looking up tables and interpolation. It not only meets the calculation accuracy, but also greatly improves the calculation speed. In 2015, Yong et al. [17] proposed water invasion diagnosis curves based on well production and pressure data for super-giant aquifer drive gas reservoirs. According to the diagnosis curves, water invasion was divided into three stages: the no aquifer influx stage, early aquifer influx stage, and middle-late aquifer influx stage. Using the same method, in 2017, they [18] proposed the diagnosis curves of water invasion in fractured-vuggy carbonate reservoirs.

Due to the existence of natural fractures in the aquifer, the traditional homogeneous models no longer meet the accuracy requirements. Therefore, many scholars have studied water invasion in dual media gas reservoirs [19–28]. Due to the more complex percolation mechanism, the statistics and numerical simulation methods are commonly used to calculate water influx. For example, Deng et al. [21] used statistical methods to obtain the nonlinear relationship between fracture height, single well fluid flux and water breakthrough time of gas wells in a fractured bottom-water reservoir, so as to predict the water breakthrough time of gas wells with different fluid flux.

For naturally fractured reservoirs, Roberto Aguilera [29] established an unsteady state water invasion model, taking the transient and pseudo-steady interporosity flow into account. They analyzed the effects of the storativity ratio and interporosity flow coefficient on dimensionless water influx curves. This provides a theoretical basis for studying the water invasion of naturally fractured gas reservoirs with edge water. However, the difference between naturally fractured aquifers and homogenous aquifers is not taken into account, and the characteristics of the dimensionless water influx curve are not obvious enough to effectively identify water invasion in naturally fractured gas reservoirs, let alone to quantify water influx in naturally fractured gas reservoirs and from a complete set of analytical methods.

From the above, we can see that an efficient method for determining water influx in naturally fractured reservoirs is still lacking. To improve this situation, based on a mathematical model of naturally fractured reservoirs, a new global search algorithm is proposed to calculate water influx. In this paper, the dimensionless water influx derivative is first proposed. With the double logarithmic curves of dimensionless water influx and its derivative, namely the characteristic curves, the flow regimes of water invasion can be identified. Then the water invasion trend can be predicted according to the water invasion curves, which provide reference for designing a reasonable gas well production system and adjusting the development plan. Following that, a sensitivity study of the characteristic curves is performed.

Furthermore, based on the sensitivity study and material balance equation, a new global search algorithm is proposed to calculate water influx. An actual field application is performed to show the accuracy and applicability of the new method, which provides a good reference for further work on the determination of water influx.

2. Conceptual Model

The aquifer of the naturally fractured gas reservoir includes two domains: matrix and natural fractures. In this model, the gas reservoir is regarded as a "well", and the water influx is the fluid flux of the "well". The assumptions for the water invasion model are as follows. The specific schematic diagram is shown in Figure 1.

1. The formation is equal-thick, circular and finite.
2. The fluid in the aquifer is single-phase, slightly compressible and isothermal, observing Darcy's law. The vertical flow of the fluid is ignored.
3. Interflow from matrix to "wellbore" (gas reservoir) is neglected, because matrix permeability in the model is much lower than fracture permeability.

4. The initial aquifer pressure is p_i, the aquifer thickness is h, the gas reservoir radius is r_g, and the aquifer radius is r_e.
5. The interporosity flow from natural fractures to the matrix is in the transient state in the aquifer.
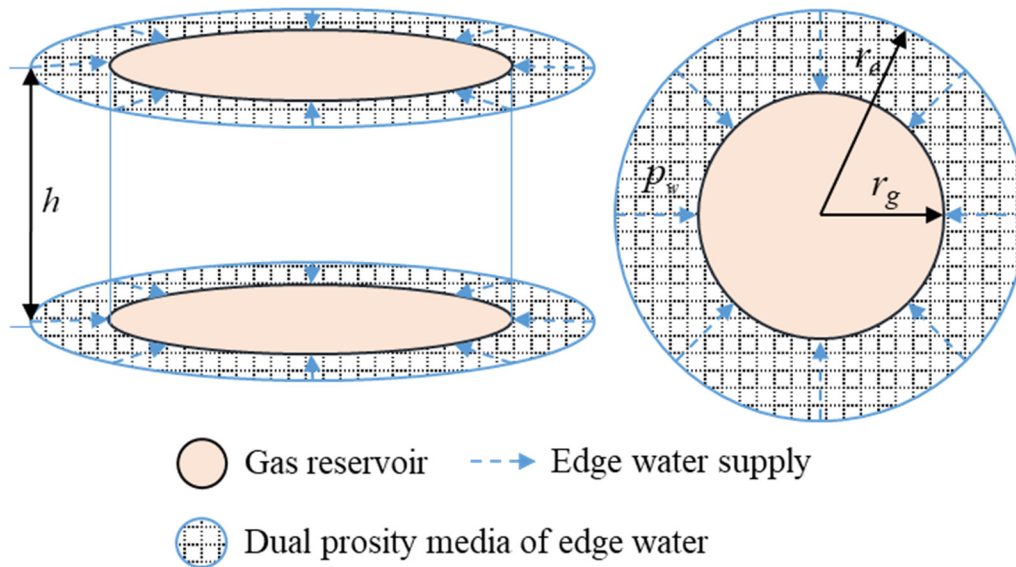

Figure 1. Naturally fractured edgewater gas reservoir. The dual porosity media of edge water is described by the Warren and Root model [30].

3. Mathematical Model

Based on the above conceptual model, a mathematical model of water invasion is established [29], which provides the theoretical base for methodology development of the water-influx determination. Taking the transient state interporosity flow in the aquifer into account, the dimensionless radial seepage equation of finite edge water is obtained.

$$\frac{\partial p_{fD}}{\partial r_D^2} + \frac{1}{r_D}\frac{\partial p_{fD}}{\partial r_D} = \omega\frac{\partial p_{fD}}{\partial t_D} + \frac{\lambda}{3}\frac{\partial p_{mD}}{\partial t_D} \tag{1}$$

The seepage equation in the matrix system satisfies

$$\frac{\partial^2 p_{mD}}{\partial t_D^2} = 3(\frac{1-\omega}{\lambda})\frac{\partial p_{mD}}{\partial t_D} \tag{2}$$

Equation (1) is the dimensionless seepage equation of the fracture with transient state interporosity flow, and Equation (2) is the dimensionless seepage equation of the matrix with transient state interporosity flow. p_{fD} is the fracture pressure in the aquifer (dimensionless); p_{mD} is the matrix pressure in the aquifer (dimensionless); r_D is the edge water radius (dimensionless); ω is the storativity ratio in the aquifer (dimensionless); λ is the interporosity flow coefficient in the aquifer (dimensionless); and t_D is time (dimensionless). Subscript "D" tables dimensionless.

Initial conditions in the edge water:

$$p_{fD}(r_D, 0) = p_{mD}(r_D, 0) = 0 \tag{3}$$

Equation (3) shows that at the initial conditions, the pressure of the fracture and matrix are the same.

The internal boundary conditions in the edge water are given by:

$$\left.\frac{\partial p_{fD}}{\partial r_D}\right|_{r_D=1} = -1(t_D > 0) \tag{4}$$

Equation (4) shows that at the interface between the gas reservoir and the edge water (internal boundary), edge water flows into the internal gas reservoir at a constant flux.

The external boundary conditions in the edge water are given by:

$$\left.\frac{\partial p_{fD}}{\partial r_D}\right|_{r_{eD}} = 0(t_D > 0) \tag{5}$$

Equation (5) shows that the external boundary of the edge water is a closed boundary and there is no fluid inflow outside.

The dimensionless variables are as follows. Dimensionless pressure is

$$p_D(r_D, t_D) = \frac{K_f h}{1.842 \times 10^{-3} q \mu_w B_w} [p_i - p(r,t)] \tag{6}$$

Dimensionless radius is

$$r_D = \frac{r}{r_g} \tag{7}$$

Dimensionless time is

$$t_D = \frac{3.6 K_f t}{[(\phi c_t)_f + (\phi c_t)_m] \mu_w r_g^2} \tag{8}$$

The storativity ratio is

$$\omega = \frac{(\phi c_t)_f}{(\phi c_t)_f + (\phi c_t)_m} \tag{9}$$

The interporosity flow coefficient is

$$\lambda = \alpha \frac{K_m}{K_f} r_g^2 \tag{10}$$

$$\alpha = \frac{4n(n+2)}{L^2} \tag{11}$$

where q is the fluid flux (m³/d); B_w is the water volume factor (m³/m³); r is the radius (m); r_e is the edge water radius; r_g is the gas reservoir radius (m); K is the permeability (darcy); p is the formation pressure (MPa); t is time (hours); ϕ is porosity (fraction); c_t is comprehensive compressibility (MPa^{-1}); μ_w is water viscosity (mPa·s); α is the form factor (dimensionless); n is the group number of orthogonal fractures, that is, the dimension of the fracture surface (integer); and L is the characteristic length of the rock, i.e., the ratio of the volume of the matrix block to its surface area (m). Subscript "*m*" tables matrix; subscript "*f*" tables fractures.

Roberto Aguilera [29] presented an exhaustive compilation of the detailed solutions by using a Laplace transform, and got the results as follows.

$$\bar{p}_{fD} = \frac{1}{s^{3/2}} \frac{1}{\sqrt{f(s)}} \frac{M}{N} \tag{12}$$

where

$$f(s) = \omega + \sqrt{\frac{\lambda(1-\omega)}{3s}} \tanh\left(\sqrt{\frac{3(1-\omega)s}{\lambda}}\right) \tag{13}$$

$$M = I_1\left(r_{eD}\sqrt{sf(s)}\right)K_0\left(r_D\sqrt{sf(s)}\right) + I_0\left(r_D\sqrt{sf(s)}\right)K_1\left(r_{eD}\sqrt{sf(s)}\right) \tag{14}$$

$$N = I_1\left(r_{eD}\sqrt{sf(s)}\right)K_1\left(\sqrt{sf(s)}\right) + I_1\left(\sqrt{sf(s)}\right)K_1\left(r_{eD}\sqrt{sf(s)}\right) \tag{15}$$

where s is the Laplace space operator (dimensionless); $I_0(x)$ are Bessel functions of the first type of zero order (dimensionless); $I_1(x)$ are Bessel functions of the first type of one order (dimensionless); $K_0(x)$ are Bessel functions of the second type of zero order (dimensionless); and $K_1(x)$ are Bessel functions of the second type of one order (dimensionless).

According to the study of Everdingen and Hurst in 1949 [1], when $r_D = 1$, the relationship between water influx and pressure is:

$$\frac{1}{s^2} = s\overline{W}_{eD}(r_D = 1)\overline{p}_{fD}(r_D = 1) \tag{16}$$

where W_{eD} is dimensionless water influx in the time domain (dimensionless); and $\overline{W}_{eD}$ is dimensionless water influx in the Laplace domain (dimensionless). With the relationship between water influx and pressure (Equation (16)), the dimensionless water influx solutions of a finite aquifer, infinite edge water, and fan-shaped gas reservoir can be obtained as follows:

(1) The dimensionless water influx in the Laplace domain of a finite aquifer is

$$\overline{W}_{eD} = \frac{\sqrt{f(s)}}{s^{3/2}}\frac{N}{M|_{r_D=1}} \tag{17}$$

(2) For infinite edge water, the outer boundary condition is

$$p_{fD}(r_D \to \infty, t_D) = p_{mD}(r_D \to \infty, t_D) = 0(t_D > 0) \tag{18}$$

Its seepage equations, initial conditions, and inner boundary conditions are consistent with the finite aquifer. Thus, the dimensionless water influx in the Laplace domain can be obtained by

$$\overline{W}_{eD} = \frac{\sqrt{f(s)}}{s^{3/2}}\frac{K_1\left(\sqrt{sf(s)}\right)}{K_0\left(\sqrt{sf(s)}\right)} \tag{19}$$

(3) The single-pore aquifer is a special case of this model, where $f(s) = 1$. The dimensionless water influx in the Laplace domain of a fan-shaped gas reservoir is

$$\left(\overline{W}_{eD}\right)_\theta = \overline{W}_{eD} \times \frac{\theta}{360°} \tag{20}$$

where θ is the angle of water invasion in the gas reservoir in degrees (°).

Finally, with Stehfest numerical inversion [31], the solution of dimensionless water influx W_{eD} in the time domain can be obtained.

4. Results and Discussions

This section involves flow regime identification and the sensitivity study based on the dimensionless water influx solutions, which provide a theoretical base for methodology development of the water influx determination.

4.1. Flow Regimes

As it is difficult to accurately identify flow regimes of water invasion according to the double logarithmic curve of dimensionless water influx, the double logarithmic curve of dimensionless water influx derivative is firstly introduced, and the water influx derivative is defined as:

$$W_{eD}' = \frac{dW_{eD}}{d \ln t_D} = t_D \frac{dW_{eD}}{dt_D} \tag{21}$$

Without loss of generality, take $r_{eD} = 5$, $\omega = 0.01$, $\lambda = 10^{-6}$. The double logarithmic curves of dimensionless water influx and their derivatives, as the characteristic curves of the water invasion model, are as follows.

In Figure 2, the flow regimes of water invasion in a naturally fractured gas reservoir with edge water can be identified in detail:

Regime I in Figure 2: Fracture radial flow. In this period, only the fluid in natural fractures flows toward the gas reservoir.

Regime II in Figure 2: Cross flow. "V-shape" caused by matrix supply. During depletion in natural fractures, the fracture pressure reduces over time. Once it reaches a certain value, the fluid within the matrix will enter into natural fractures.

Regime III in Figure 2: Transitional radial flow. The fluid flows from the matrix to natural fractures, and then to the gas reservoir. However, the pressure drop rate is not uniform and the flow does not reach the state of dynamic balance.

Regime IV in Figure 2: Pseudo-steady flow. The dimensionless water influx curve exhibits a horizontal line, and the flow reaches the state of dynamic balance.
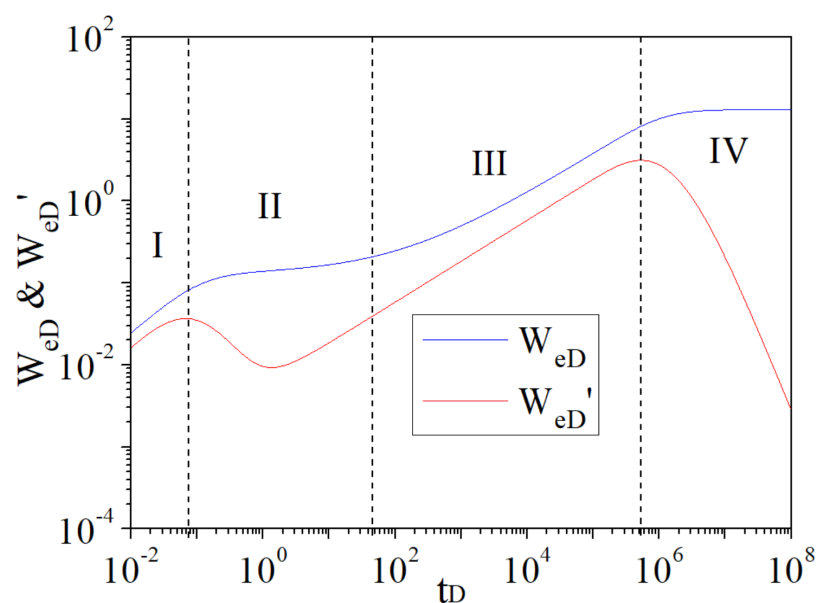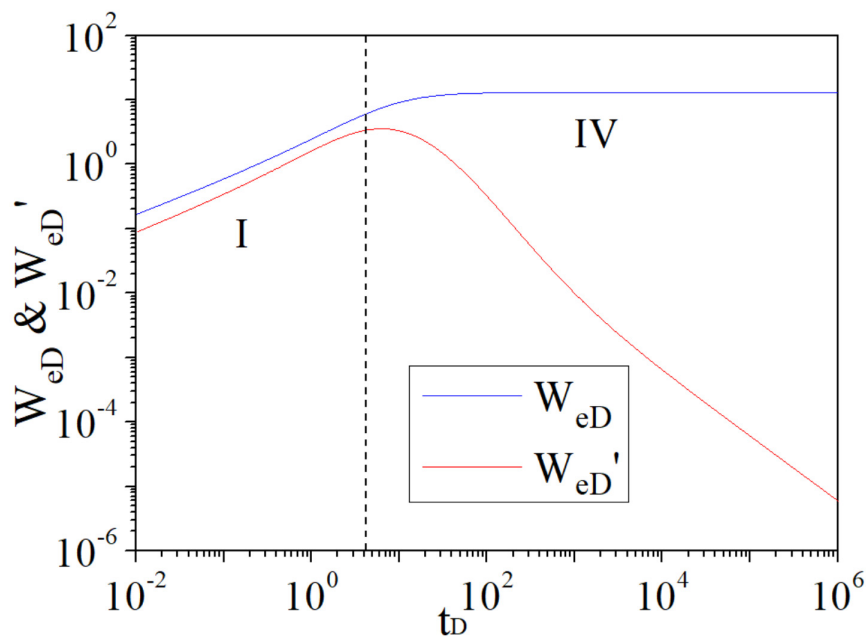

Figure 2. Dimensionless water influx characteristic curves of a naturally fractured edge water gas reservoir.

In Figure 3, the flow regimes of water invasion in a homogeneous gas reservoir with edge water can be identified in detail:

Regime I in Figure 3: Radial flow. In this period, the fluid in the matrix flows toward the gas reservoir.

Regime IV in Figure 3: Pseudo-steady flow. The dimensionless water influx curve exhibits a horizontal line, and the flow reaches the state of dynamic balance.

Figure 3. Dimensionless water influx characteristic curves of a homogeneous edge water reservoir.

Differences in water influx characteristic curves between a homogeneous gas reservoir and dual media gas reservoir: In water influx characteristic curves of the dual media water invasion model, there are four flow regimes of water invasion, the water influx curve is double stepped and the derivative curve has concave features. In water influx characteristic curves of the homogeneous water invasion model, there are only two flow regimes of water invasion, the water influx curve is single step, and the derivative curve has no concave features.

Note that a continuum will occur between the water influx curves of the homogeneous gas reservoir and dual media gas reservoir when the ratio of permeability between the matrix and fractures is 1. In that situation, the properties of naturally fractured gas reservoirs are similar to those of homogeneous gas reservoirs, and the shape of the water influx characteristic curves of the two are the same.

4.2. Sensitivity Study

In this section, the impacts of the aquifer and gas reservoir radius ratio r_{eD}, storativity ratio ω and interporosity flow coefficient λ on dimensionless water influx transient behaviors are studied.

Without loss of generality, when $\omega = 0.01$, $\lambda = 10^{-6}$, $r_{eD} = \infty$, $r_{eD} = 100$, $r_{eD} = 20$, $r_{eD} = 5$, the curves of dimensionless water influx and derivative are as follows.

In Figures 4 and 5, the smaller the aquifer and gas reservoir radius ratio r_{eD} is, the smaller the dimensionless water influx and its derivative are, and the shorter the duration of fracture radial flow (regime I) is, due to less fluid in natural fractures. Furthermore, the "V-shape" in the curve of the water influx derivative is more obvious during the cross flow (regime II). It can be deduced that the aquifer and gas reservoir radius ratio mainly controls the dimensionless water influx value and the depth of the "V-shape" in derivative curves.
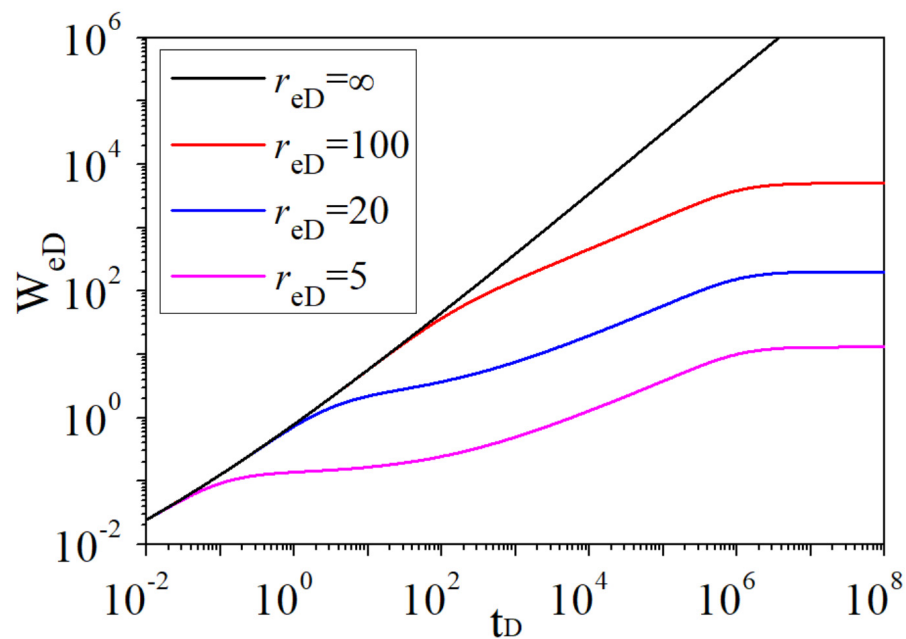
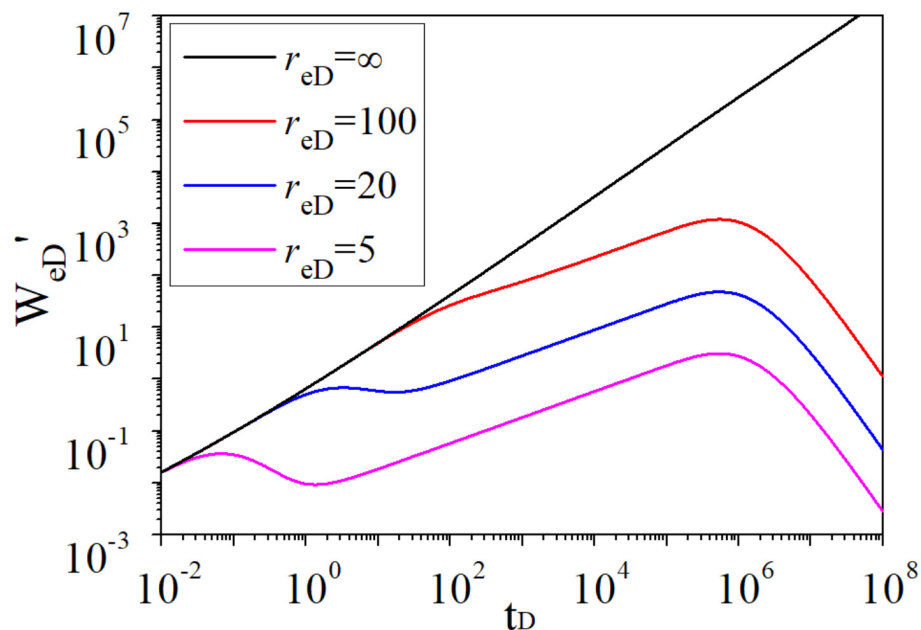**Figure 4.** Dimensionless water influx curves of different r_{eD}.

Figure 5. Dimensionless water influx derivative curves of different r_{eD}.

Without loss of generality, when $r_{eD} = 5$, $\lambda = 10^{-6}$, $\omega = 0.01$, $\omega = 0.1$, $\omega = 0.5$, the curves of dimensionless water influx and derivative are as follows.

In Figures 6 and 7, at the early stage of water invasion, the smaller the storativity ratio ω, the smaller the value of dimensionless water influx, the shorter the duration of fracture radial flow (regime I) due to less fluid in natural fractures, and the greater the difference in height between the double steps is in the dimensionless water influx curve. For derivative curves, the smaller the storativity ratio ω, the earlier the "V-shape" appears. When it comes to pseudo-steady flow, the water influx is the same and is independent of the ω.
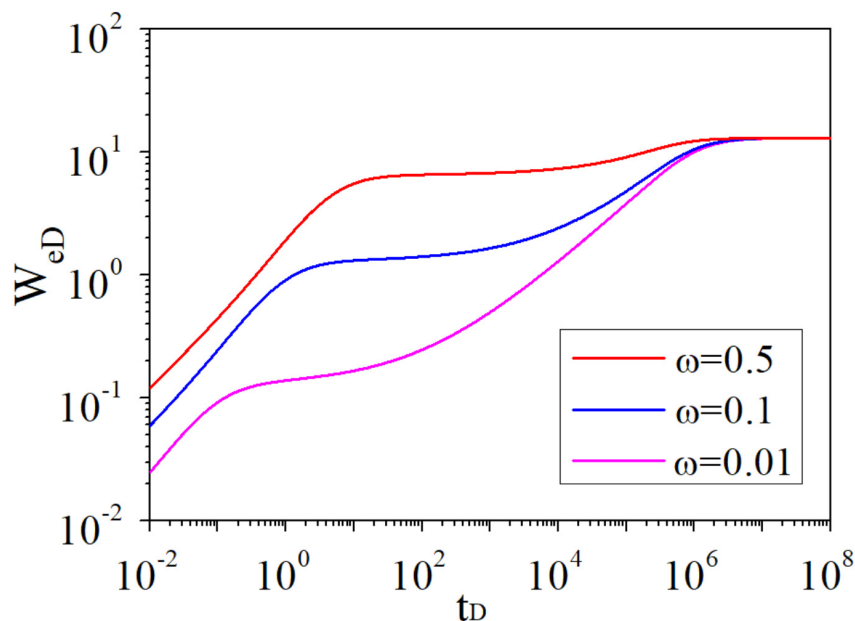
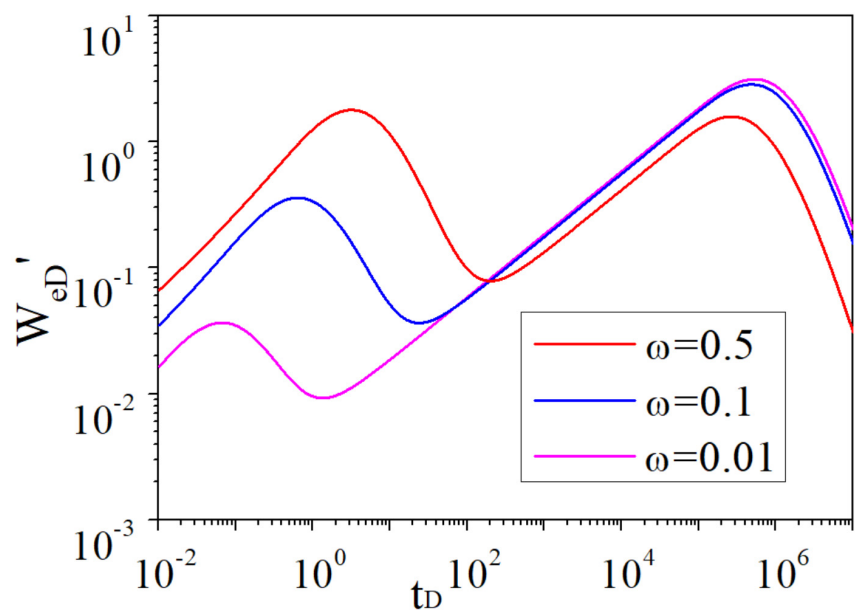**Figure 6.** Dimensionless water influx curves of different ω.

Figure 7. Dimensionless water influx derivative curves of different ω.

It can be seen that the storativity ratio ω mainly affects the two-step height of the curve of dimensionless water influx and the appearance time of the "V-shape" in the curve of the water influx derivative.

Without loss of generality, when $r_{eD} = 5$, $\omega = 0.01$, $\lambda = 10^{-9}$, $\lambda = 10^{-6}$, $\lambda = 10^{-3}$, the curves of dimensionless water influx and its derivative are as follows.

In Figures 8 and 9, the smaller the interporosity flow coefficient λ is, the longer the duration of cross flow (regime II). This is because the smaller the interporosity flow coefficient, the smaller the cross fluid flux from the matrix to fractures. As a result, the double steps in the dimensionless water influx curve and the "V-shape" in the derivative curve are more obvious.
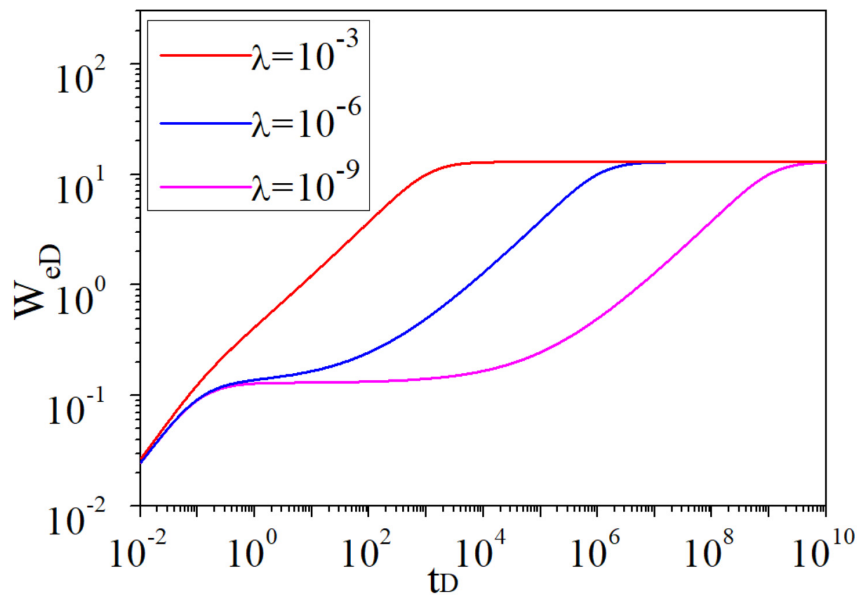
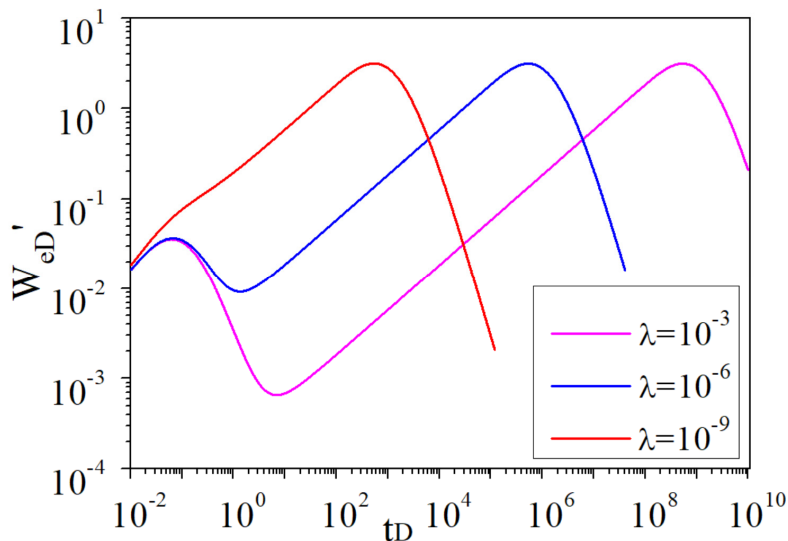**Figure 8.** Dimensionless water influx curves of different λ.

Figure 9. Dimensionless water influx derivative curves of different λ.

Thus, it can be found that the interporosity flow coefficient λ mainly influences the depth of the double steps in the dimensionless water influx curve and that of the "V-shape" in the derivative curve.

5. Methodology

Based on the above flow regime identification and sensitivity study, a new global search algorithm is proposed to calculate the water influx, and the calculated process is as follows.

(1) In general, the radius of the gas reservoir and the radius of the aquifer are unknown. Assume the value of the gas reservoir radius r_g and the aquifer and gas reservoir radius ratio r_{eD}. In addition, obtain the dimensionless parameters from the field data.

(2) Calculate the dimensionless water influx in the Laplace domain with the dimensionless parameters. With Stehfest numerical inversion [31], the solution of dimensionless water influx W_{eD} in the time domain can be obtained. The calculation details are shown as follows.

$$\overline{W}_{eD} = \frac{\sqrt{f(s)}}{s^{3/2}} \frac{N}{M|_{r_D=1}} \tag{22}$$

where

$$f(s) = \omega + \sqrt{\frac{\lambda(1-\omega)}{3s}}\tanh\left(\sqrt{\frac{3(1-\omega)s}{\lambda}}\right) \tag{23}$$

$$\begin{cases} M = I_1\left(r_{eD}\sqrt{sf(s)}\right)K_0\left(r_D\sqrt{sf(s)}\right) + I_0\left(r_D\sqrt{sf(s)}\right)K_1\left(r_{eD}\sqrt{sf(s)}\right) \\ N = I_1\left(r_{eD}\sqrt{sf(s)}\right)K_1\left(\sqrt{sf(s)}\right) + I_1\left(\sqrt{sf(s)}\right)K_1\left(r_{eD}\sqrt{sf(s)}\right) \end{cases} \tag{24}$$

(3) Obtain water influx according to the study of Everdingen and Hursr [1].

$$W_e = A_g h \phi_f c_{tf} \int_0^t \frac{\partial \Delta p}{\partial t'} W_{eD}(t-t')dt' \approx A_g h \phi_f c_{tf} \sum_{j=0}^t \Delta p_j W_{eD}\left(\Delta t_{Dj}, r_D\right) \tag{25}$$

The dimensionless water influx is derived following Everdingen and Hursr [1], and the detailed derivations were provided in their work. It is written as

$$W_{eD} = \int_0^{t_D}\left(r_D\frac{\partial p_D}{\partial r_D}\right)_{r_D=1}dt_D \tag{26}$$

Further, one can obtain

$$W_e = 2\pi r_g^2 h \phi_f c_{tf}\left[\begin{array}{c} \Delta p_0 W_{eD}\left(\left(t_j-t_0\right)_D, r_D\right) + \Delta p_1 W_{eD}\left(\left(t_j-t_1\right)_D, r_D\right) \\ +\ldots+ \Delta p_{t-1}W_{eD}\left(\left(t_j-t_{t-1}\right)_D, r_D\right) \end{array}\right] \tag{27}$$

$$\begin{cases} \Delta p_0 = p_i - \overline{p}_1 = p_i - \frac{p_i+p_1}{2} = \frac{p_i-p_1}{2} \\ \Delta p_1 = \overline{p}_1 - \overline{p}_2 = \frac{p_i+p_1}{2} - \frac{p_1+p_2}{2} = \frac{p_i-p_2}{2} \\ \Delta p_2 = \overline{p}_2 - \overline{p}_3 = \frac{p_1+p_2}{2} - \frac{p_2+p_3}{2} = \frac{p_1-p_3}{2} \\ \Delta p_{j-1} = \overline{p}_{j-1} - \overline{p}_j = \frac{p_{j-2}+p_{j-1}}{2} - \frac{p_{j-1}+p_j}{2} = \frac{p_{j-2}-p_j}{2} \end{cases} \tag{28}$$

where W_e is the water influx (m^3); W_{eD} is the dimensionless water influx (dimensionless); Δp_0 represents the pressure difference of the initial segment (MPa); Δp_1 represents the first pressure difference (MPa); Δp_2 represents the second pressure difference (MPa); and Δp_{j-1} indicates the pressure difference at the $(j-1)$th stage (MPa). They are shown in Figure 10.
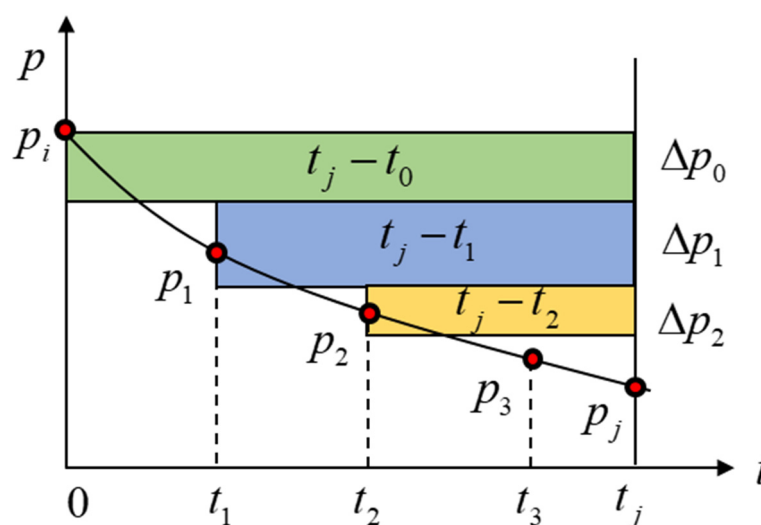

Figure 10. Pressure drop curve.

(4) Verify the results according to the material balance equation and the error between dynamic and static geological reserves. If the linear fitting correlative coefficient of the material balance curve is

greater than 0.95, and the error between dynamic and static geological reserves is less than 0.2, the results can be accepted. Otherwise, new values of the gas reservoir radius r_g and aquifer and gas reservoir radius ratio r_{eD} will be reassumed, and recalculate the water influx until the requirements are met. The material balance equation of water-drive gas reservoirs [32] is shown as follows.

$$\frac{p}{Z}(1 - c_c\Delta P - e) = \frac{p_i}{Z_i}(1 - \frac{G_p}{G}) \tag{29}$$

$$c_c = \frac{c_p + s_{wc}c_w}{1 - s_{wc}} \tag{30}$$

$$e = \frac{W}{V_{gi}} = \frac{W_e - W_p B_w}{A_g h \phi(1 - s_{wc})} \tag{31}$$

where Z is the compression factor (dimensionless); Δp represents the pressure difference (MPa); G_p is the cumulative gas flux (m^3); G is the gas reservoir dynamic geological reserves (m^3); c_c is defined as gas reservoir volume compressibility (MPa^{-1}); c_p is rock compressibility (MPa^{-1}); c_w is formation water compressibility (MPa^{-1}); s_{wc} is irreducible water saturation (fraction); e is the volume coefficient of stored water, that is, the percentage of water volume left in the volume of gas reservoir (fraction); We is the water influx (m^3); Wp is the cumulative water flow flux on the ground (m^3); and W is the volume of the water left in the formation (m^3). Define the H pressure of the gas reservoir as p_H.

$$p_H = \frac{p}{Z}(1 - c_c\Delta p - e) \tag{32}$$

$$p_{Hi} = \frac{p_i}{Z_i} \tag{33}$$

where p_{Hi} is the H pressure of the gas reservoir under original conditions (MPa). Then the material balance equation for water-drive gas reservoirs becomes:

$$p_H = p_{Hi}(1 - \frac{G_p}{G}) \tag{34}$$

The material balance curve of p_H and G_p is used to verify the accuracy of the gas reservoir radius r_g and aquifer and gas reservoir radius ratio r_{eD} and water influx, which is shown in Figure 11.
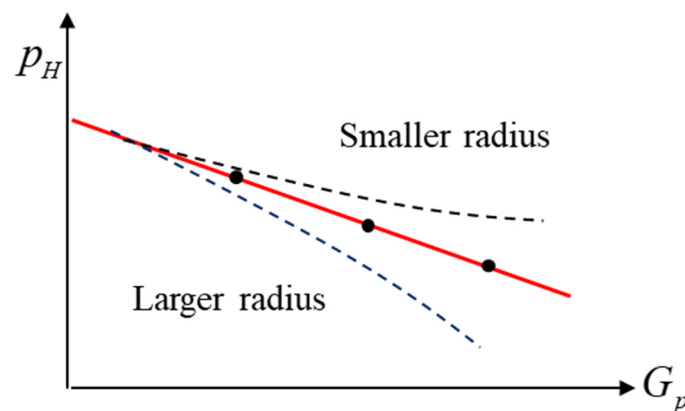

Figure 11. Validation results by the material balance equation.

If the linear fitting correlative coefficient of the material balance curve of p_H and G_p is greater than 0.95, the linear regression equation of the p_H and G_p can be obtained.

$$p_H = a + bG_p \tag{35}$$

where a and b are constants (dimensionless). The dynamic geological reserves of gas reservoir G are obtained.

$$G = \left| \frac{a}{b} \right| \tag{36}$$

where G is the dynamic geological reserve of the gas reservoir (m^3).

The static geological reserves G_s are calculated according to the volume method.

$$B_g = \frac{p_{sc}}{Z_{sc} T_{sc}} \frac{ZT}{p} \tag{37}$$

$$G_s = \frac{2\pi r_g^2 h \phi (1 - s_{wc})}{B_g} \tag{38}$$

where B_g is the gas volume factor (m^3/m^3); G_s is the static geological reserve of the gas reservoir, (m^3); T is the gas reservoir temperature (K). Subscript "*sc*" tables ground conditions.

The error between dynamic and static geological reserves is

$$\Delta\delta = \frac{G_s - G}{G} \tag{39}$$

where $\Delta\delta$ is the error between dynamic and static geological reserves (decimal).

(6) Obtain the dimensionless water invasion characteristic curves according to the value of the gas reservoir radius r_g and aquifer and gas reservoir radius ratio r_{eD}. Then, combined with dimensionless time, the flow regime of water invasion can be identified.

6. Field Application

In this section, a naturally fractured edge water gas reservoir Z1 was chosen for field application by using the proposed methodology.

The data of the reservoir and fluid are collected in Table 1, and its production dynamic data is shown in Table 2. In Table 1, the reservoir thickness, irreducible water saturation, and porosity are obtained by well logging. The formation water viscosity, formation water volume coefficient, pseudo-critical pressure, pseudo-critical temperature, and formation water compressibility are measured by PVT (pressure vs. temperature) experiments. Rock compressibility can be obtained by the rock compression test. The storativity ratio, initial formation pressure, initial formation temperature, natural fracture permeability, and matrix permeability are acquired by the well test.

Table 1. Data parameters of gas reservoir Z1.

| Parameters	Values	Units
Reservoir thickness	27	m
Irreducible water saturation	0.32	decimal
Formation water viscosity	0.45	mPa·s
Formation water volume coefficient	1.01	m^3/m^3
Storativity ratio	0.1	dimensionless
Interporosity flow coefficient	10^{-6}	dimensionless
Pseudo-critical pressure	4.67	MPa
Pseudo-critical temperature	195.15	K
Initial formation pressure	29.7	MPa
Initial formation temperature	364.15	K
Porosity	0.1	decimal
Natural fracture permeability	1	mD
Matrix permeability	0.01	mD
Formation water compressibility	0.0046	MPa^{-1}
Rock compressibility	0.000435	MPa^{-1}

Table 2. Production dynamic data of gas reservoir Z1.

t/mon	p/MPa	$Gp/10^8$ m^3	$Wp/10^4$ m^3
0	29.7	0	0
12	27.4	6.88	0
20	25	17	120
28	23.7	27.5	180
36	21.3	37.3	260.7
48	19.4	51.5	500
60	17.6	61.6	1050

Where bot G_p is the cumulative gas flux (10^8 m^3); and W_p is the cumulative water flux (10^4 m^3). According to the statistical formula, the compression factor Z is calculated.

$$Z = 1 - \frac{3.52p_r}{10^{0.9813T_r}} + \frac{0.274p_r^2}{10^{0.8157T_r}} \tag{40}$$

where Z is the compression factor (dimensionless); p_r is pseudo reduced pressure (dimensionless); and T_r is the pseudo reduced temperature (dimensionless).

The new global search algorithm is used to calculate water influx. Set the value of r_g to 100, 200, ..., 5000, and the value of r_{eD} is 1, 2, ..., 40. After 2000 iterations, the optimal gas reservoir radius r_g is found to be 3600 m, and the optimal aquifer and gas reservoir radius ratio r_{eD} is 2. The material balance curve of p_H and G_p is used to verify the results, which are shown in Figure 12.

$Gp = -0.1742P_H + 28.87$

$R^2 = 0.9838$
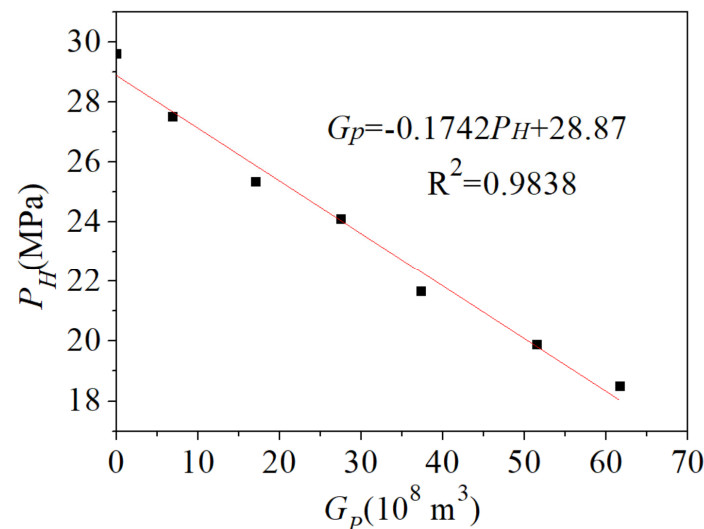
Figure 12. Validation results by the material balance equation of gas reservoir Z1.

The correlative coefficient of linear fitting is 0.9838, which meets the requirement. Combined with the linear regression equation, the dynamic geological reserves of gas reservoir G are obtained.

$$G = \frac{28.87}{0.1742} = 165.7(10^8 \text{ m}^3) \tag{41}$$

The static geological reserves G_s are calculated according to the volume method.

$$B_g = \frac{p_{sc}}{Z_{sc}T_{sc}} \frac{ZT}{p} = 0.004236(\text{m}^3/\text{m}^3) \tag{42}$$

$$G_s = \frac{2\pi r_g^2 h\phi(1 - s_{wc})}{B_g} = 174.1(10^8 \text{ m}^3) \tag{43}$$

The error between dynamic and static geological reserves is

$$\Delta\delta = \frac{G_s - G}{G} = 0.0507 \tag{44}$$

where $\Delta\delta$ is the error between dynamic and static geological reserves (decimal). The error meets the engineering requirement, and the results are accepted. Therefore, the gas reservoir radius r_g is 3600 m, and the aquifer and gas reservoir radius ratio r_{eD} is 2. Furthermore, water influx and corresponding dimensionless time can be obtained as shown in Table 3.

Table 3. Water influx of gas reservoir Z1.

$We/10^4$ m^3	t_D	p_H
0.00	0.000	29.62
0.39	0.011	27.51
1.17	0.018	25.37
2.09	0.025	24.14
3.18	0.032	21.71
4.99	0.042	19.96
6.88	0.053	18.63

The water invasion characteristic curves can be obtained, which are shown in Figure 13.
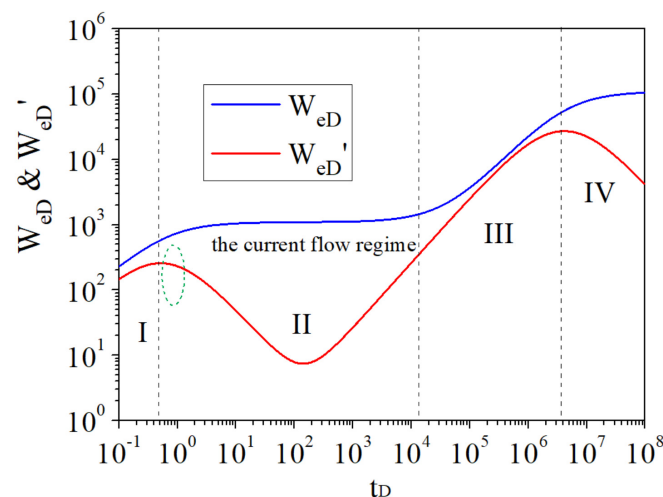

Figure 13. Dimensionless water invasion characteristic curves of gas reservoir Z1. Regime I is fracture radial flow. Regime II is cross flow caused by matrix supply. Regime III is transitional radial flow. Regime IV is pseudo-steady flow.

According to the dimensionless time and water invasion characteristic curves of gas reservoirs, it can be judged that the flow regime of the gas reservoir is the early state of cross flow and the water influx is small. If the gas flow flux is too large to make water influx increase sharply, it is probable that the gas well will be flooded. At this time, a reasonable gas well production working system is needed to extend the dry production time and improve gas reservoir recovery.

7. Conclusions

In this paper, a dimensionless water influx derivative curve is first introduced, which is used to identify flow regimes of water invasion. Then, a sensitivity analysis is performed to study the impacts of key factors on flow regimes, including formation pore type, the aquifer and gas reservoir radius ratio, the storativity ratio, and the interporosity flow coefficient. Based on the sensitivity study and

material balance equation, a new method for determining water influx in naturally fractured reservoirs is developed. Some important conclusions are drawn:

1. After analyzing the water influx characteristic curves of naturally fractured reservoirs, there are four flow regimes, the water influx curves are double stepped and a "V-shape" appears in the derivative curves. For the water influx characteristic curves of homogeneous reservoirs, there are only two flow regimes, the water influx curves are single stepped and the derivative curves have no "V-shape".

2. With the decrease in the storativity ratio ω, the "V-shape" in the derivative curve appears earlier, and the difference in height between the double steps in the dimensionless water influx curve is greater.

3. The smaller the interporosity flow coefficient λ is, the more obvious the double steps in the dimensionless water influx curve and the more apparent the "V-shape" in the derivative curve are.

4. The smaller the aquifer and gas reservoir radius ratio r_{eD} is, the more obvious the "V-shape" in the curve of the water influx derivative during the cross flow is, and the smaller the dimensionless water influx and its derivative are. These features provide meaningful tools to quantify the water influx.

5. Water influx, gas radius, aquifer radius, dynamic geological reserves, and the regime of water invasion can be obtained by the global search algorithm. The results from the case study were verified by analyzing the error between dynamic and static geological reserves, and the error met the engineering accuracy, which indicates that the accuracy of the proposed method is acceptable.

This is our primary work about water influx, and more efforts will be made to focus on (1) incorporation of other approaches, like automatic inversion, and (2) global sensitivity analysis [33] to avoid a risk of loss of generality, and (3) type-curve matching by using the water influx curves.

Nomenclatures

B_w	water volume factor, m^3/m^3
B_g	gas volume factor, m^3/m^3
c_p	rock compressibility, MPa^{-1}
c_w	formation water compression coefficient, MPa^{-1}
c_t	comprehensive compression coefficient, MPa^{-1}
c_c	gas reservoir volume compression coefficient, MPa^{-1}
s_{wc}	irreducible water saturation, dimensionless
h	formation thickness, m
K	permeability, darcy
p	pressure, MPa
p_i	initial formation pressure, MPa
q	flow flux, m^3/d

r_e	edge water radius, m
r_g	gas reservoir radius, m
r	radial distance, m
t	time, hour
α	form factor, dimensionless
n	the number of orthogonal fracture groups, integer
L	the characteristic length of the rock, m
W_e	water influx, m^3
W_{eD}	dimensionless water influx, dimensionless
Wp	the cumulative water flow flux in the ground, m^3
s	Laplace space operator, dimensionless
θ	the angle of water invasion in reservoirs, degree (°)
$I_0(x)$	modified Bessel function (one class, zero order)
$I_1(x)$	modified Bessel function (one class, first order)
$K_0(x)$	modified Bessel function (second class, zero order)
$K_1(x)$	modified Bessel function (second class, first order)
Δp_j	the pressure difference at the jth stage, MPa
Z	compression factor, dimensionless
Gp	cumulative gas flow flux, m^3
G	gas reservoir dynamic geological reserves, m^3
Gs	static geological reserves of gas reservoir, m^3
W	the volume of the left water in the formation, m^3
p_H	the H pressure of gas reservoirs, MPa
p_{Hi}	the gas reservoir H pressure under original conditions, MPa
e	the percentage of stored water volume in the volume of the gas reservoir, dimensionless
a, b	constants, dimensionless
T	gas reservoir temperature, K

Greek

μ_w	water viscosity, mPa·s
ϕ	porosity, decimal
ω	storativity ratio in aquifer, dimensionless
λ	interporosity flow coefficient in aquifer, dimensionless
$\Delta\delta$	the error between dynamic and static geological reserves, decimal
p_r	pseudo reduced pressure, dimensionless
T_r	pseudo reduced temperature, dimensionless

Subscript

D	dimensionless
m	matrix
f	fracture
w	formation water
g	gas
sc	ground condition

Superscript

−	Laplace transform

SI Conversion Factors

MPa	$\times 1.0 \times 10^6$ = Pa
h	$\times 3.6 \times 10^3$ = s
mPa·s	$\times 1.0 \times 10^{-3}$ = Pa·s
millidarcy	$\times 1 \times 10^{-3}$ = Darcy
Darcy	$\times 1 \times 10^{-12}$ = m^2

References

1. Van Everdingen, A.F.; Hurst, W. The Application of the Laplace Transformation to Flow Problems in Reservoirs. *Soc. Pet. Eng.* **1949**, *1*, 305–324. [CrossRef]

2. Fetkovich, M.J. A Simplified Approach to Water Influx Calculations-Finite Aquifer Systems. *Soc. Pet. Eng.* **1971**, *23*, 814–824. [CrossRef]

3. Hu, J.; Li, X.; Jing, W.; Xiao, Q. A New Method for Determining Dynamic Reserves and Water Influx in Water Drive Gas Reservoir. *Xinjiang Pet. Geol.* **2012**, *33*, 720–722.

4. Liao, Z. Analysis of Outflow Rules and Production Dynamics of Fractured Water-drive Gas Reservoirs. Master's Thesis, Southwest Petroleum University, Chengdu, Sichuan, China, 2016.

5. Liao, Z.; Li, J. Review of Typical Calculation Methods for Water Influx of Water Drive Gas Reservoirs. *Petrochem. Technol.* **2016**, *23*, 117–118.

6. Liu, S.; Li, Z.; Chen, P.; Guo, C.; Lai, F. A New Method for Calculating the Aquifer Influx of Abnormal High-pressure Gas Reservoirs. *Spec. Oil Gas Reserv.* **2017**, *24*, 139–142.

7. Liu, T.; Huang, Q. Several Methods to Calculate Water Influx of Water Drive Gas Reservoir. *Petrochem. Ind. Technol.* **2016**, *23*, 116–125.

8. Lu, K. A New Method for Water Invasion Prediction and Dynamic Reserves Calculation of Gas Cap Reservoirs. *Spec. Oil Gas Reserv.* **2017**, *24*, 89–93.

9. Shimada, M.; Yildiz, T. Predicting Water Influx from Common Aquifers. In Proceedings of the EUROPEC/EAGE Conference and Exhibition, Amsterdam, The Netherlands, 8–11 June 2009.

10. Song, D.; Li, X.; Nie, Y.; Xu, B. Review of Calculation Methods for Water Influx of Water Drive Gas Reservoirs. *West China Explor. Eng.* **2011**, *23*, 75–78.

11. Xia, J.; Zheng, L. Calculation Method for Water Influx of Edge Water Gas Reservoir with Oil Ring. *J. Liaoning Shihua Univ.* **2017**, *37*, 30–34.

12. Xu, G.; Zhu, C. Research of water production model in water encroachment gas deposit. *Inn. Mong. Petrochem.* **2011**, *37*, 172–173.

13. Yu, Q.; Mou, Z.; Liu, P.; Li, Y.; Xia, J.; Li, B. Calculation Methods of Water Influx in Gas Reservoirs with Aquifers. *Xinjiang Pet. Geol.* **2017**, *38*, 586–591.

14. Mcewen, C.R. Material Balance Calculations with Water Influx in the Presence of Uncertainty in Pressures. *Soc. Pet. Eng.* **1962**, *2*, 120–128. [CrossRef]

15. Al-Ghanim, J.A.; Nashawi, I.S.; Malallah, A. Prediction of Water Influx of Edge-Water Drive Reservoirs Using Nonparametric Optimal Transformations. In Proceedings of the North Africa Technical Conference and Exhibition, Cairo, Egypt, 20–22 February 2012.

16. Kryuchkov, S.; Moon, D.; Kantzas, A. Micro-CT Investigation of Water Influx. In Proceedings of the Canadian International Petroleum Conference, Calgary, AB, Canada, 12–14 June 2007.

17. Li, Y.; Li, B.; Xia, J.; Zhang, J.; Wang, D.; Zhu, Z.; Xiao, X. New Method of Water Influx Identification and Ranking for a Super-Giant Aquifer Drive Gas Reservoir. In Proceedings of the SPE Oil & Gas India Conference and Exhibition, Mumbai, India, 24–26 November 2015.

18. Li, Y.; Jia, C.; Peng, H.; Li, B.; Liu, Z.; Wang, Q. Method of Water Influx Identification and Prediction for a Fractured-Vuggy Carbonate Reservoir. In Proceedings of the SPE Middle East Oil & Gas Show and Conference, Manama, Bahrain, 6–9 March 2017.

19. Chen, H.; Du, J.; Guo, P.; Liu, D.; Xiao, F.; Yang, Z. Study on Calculation of Dynamic Reserves and Water Influx in Fractured Condensate Gas Reservoir. *Lithol. Reserv.* **2012**, *24*, 117–120.

20. Chen, J.; Yan, Y.; Zhang, A. Method for predicting water invasion in fractured gas reservoirs with water. *Spec. Oil Gas Reserv.* **2010**, *17*, 66–68, 123–124.

21. Deng, Y.; Li, S.; Li, J. Water Invasion Performance of Fractured Gas Reservoir with Bottom-Aquifer. *Spec. Oil Gas Reserv.* **2016**, *23*, 93–95, 155.

22. Li, X.; Zhang, D. *Mathematical Method and Well Testing Mathematical Model*; Petroleum Industry Press: Beijing, China, 1993; Volume 11, pp. 27–35, 61–96.

23. Lu, D. *Modern Well Test Theory and Application*; Petroleum Industry Press: Beijing, China, 2009; Volume 1, pp. 44–50, 79–84, 226–246, 260–261.

24. Sun, W.; Wang, S.; Yang, H.; Liu, L. Material Balance Method of Fractured Water Drive Reservoirs Considering Water Invasion Intensity. *Pet. Geol. Recovery Effic.* **2009**, *16*, 85–87, 117.

25. Yang, L.; Wang, Y.; Wang, Z.; Huang, T.; Zhu, Q. Strength Estimate and the Volume Calculation for Water approaching of the Fractured Gas Reservoirs. *West China Explor. Eng.* **2011**, *23*, 43–46, 50.

26. Yang, Y.; Feng, W.; Song, C. Computation Theory of Aquifer Influx in fractured edge-water drive reservoir. *J. Mineral. Petrol.* **2001**, *21*, 79–81.

27. Zhou, Y.; Meng, Y.; Xu, Z.; Wang, Y.; Liang, H.; Li, G.; Zhou, H.; Wen, C. Study on the Impact of Fracture Density on the Law of Water Invasion in Tight Sandstone Gas Reservoirs. *J. Chongqing Univ. Sci. Technol. Nat. Sci. Ed.* **2015**, *17*, 13–17.

28. Zhu, Z. Study on the Dynamic Law of Water Invasion of Fractured Bottom Water Gas Reservoirs. Master's Thesis, Southwest Petroleum University, Chengdu, Sichuan, China, 2016.

29. Aguilera, R. Unsteady State Water Influx in Naturally Fractured Reservoirs. In Proceedings of the Annual Technical Meeting, Petroleum Society of Canada, Calgary, AB, Canada, 12–16 June 1988.

30. Warren, J.E.; Root, P.J. The behavior of naturally fractured reservoirs. *SPE J.* **1963**, *3*, 245–255. [CrossRef]

31. Stehfest, H. Algorithm 368: Numerical Inversion of Laplace Transforms. *Commun. ACM* **1970**, *13*, 47–49. [CrossRef]

32. Li, C. *Fundamentals of Reservoir Engineering*, 2nd ed.; Petroleum Industry Press: Beijing, China, 2011; Volume 9, pp. 174–184.

33. Park, J.; Yang, G.; Satija, A.; Scheidt, C.; Caers, J. DGSA: A Matlab toolbox for distance-based generalized sensitivity analysis of geoscientific computer experiments. *Comput. Geosci.* **2016**, *97*, 15–29. [CrossRef]